

Roche limit and stellar disruption in the Simpson–Visser spacetime

Marcos V. de S. Silva^{1,*}

¹*Department of Theoretical Physics, Atomic and Optics, Campus Miguel Delibes, University of Valladolid UVA, Paseo Belén, 7, 47011 - Valladolid, Spain*

(Dated: January 23, 2026)

Due to the tidal forces that a black hole can produce, certain types of compact objects may undergo disruption as they approach the black hole. This disruption point is known as the Roche limit (or Roche radius). In this work, we studied the tidal forces arising from the presence of the Simpson–Visser black bounce. We analyzed the tidal forces both for a static observer and for a radially infalling observer and showed that differences arise depending on the choice of observer. We used the tidal forces together with the stellar binding forces to determine the Roche radius for neutron stars, white dwarfs, and Sun-like stars, and to investigate how the Simpson–Visser regularization affects the tidal disruption of these astrophysical objects. We also examined whether, for astrophysical black holes such as M87* and Sgr A*, these stellar disruption processes occur inside or outside the event horizon, and thus whether they are observable.

I. INTRODUCTION

The detection of black hole shadows represents an important point in observational astrophysics and provides a direct probe of the strong-field regime of gravity [1, 2]. Using very-long-baseline interferometry at millimeter wavelengths, the Event Horizon Telescope (EHT) collaboration achieved the first images of the shadow of the supermassive black hole as the M87* and Sgr A* [1–5]. These observations revealed a dark central region surrounded by a bright emission ring, consistent with theoretical predictions for photon capture by a black hole and gravitational lensing near the event horizon. The measured size and shape of the shadows agree with the expectations of general relativity, allowing stringent tests of Einstein’s theory in the strong-gravity regime and placing constraints on alternative models of compact objects [6]. In addition, shadow observations provide valuable information about black hole masses, distance from the black hole, spins, and the properties of the surrounding accretion flows [6].

The detection of gravitational waves and black hole shadows has strongly reinforced the theoretical prediction of black holes, since the astrophysical observations are in remarkable agreement with the theoretical expectations for these objects [7–13]. Despite this compelling evidence, neither shadow observations nor gravitational-wave detections constitute definitive proof of the existence of black holes, as other theoretical models can mimic similar signatures in certain regimes [14, 15]. Alternative compact objects, such as gravastars, boson stars, or wormholes, may reproduce features of the gravitational-wave signals or the optical appearance of black hole shadows [11, 13, 14, 16–19]. Therefore, although current observations provide strong support for the black hole paradigm, a complete and unambiguous identification still requires further observational tests ca-

pable of discriminating between black holes and these exotic alternatives.

An alternative to standard black holes is provided by regular black holes [20]. These compact objects possess an event horizon, as in the usual black hole case, but differ by not containing singularities. In the context of general relativity, regular black holes are not vacuum solutions and require nonstandard matter sources that violate the energy conditions in order to be sustained, such as nonlinear electrodynamics, scalar fields, dark matter, and other fields [21–25]. The first regular black hole solution was proposed by Bardeen and later interpreted by Ayón-Beato and García as a solution of Einstein’s equations sourced by nonlinear electrodynamics [26, 27]. Since then, many regular black hole models have been proposed and extensively studied in the literature [28–37].

Another class of regular solutions is provided by the so-called black bounces. These models, originally proposed by Hochberg and Visser and later studied in greater detail by Simpson and Visser [38, 39], are characterized by the presence of a wormhole throat hidden behind an event horizon. One of the most prominent black bounce models is the Simpson–Visser solution [39]. This model arises from a regularization procedure applied to the Schwarzschild metric, in which the central singularity and its neighborhood are removed and replaced by a wormhole throat [40, 41]. Within general relativity, this solution was initially obtained by considering a minimal coupling between a phantom scalar field and nonlinear electrodynamics [42–44]. It is also possible to reproduce this solution by considering linear electrodynamics with a nonminimal coupling to the scalar field, or within alternative theories of gravity [45–48]. Since the original work of Simpson and Visser, many other black bounce models have been proposed and investigated in a variety of contexts, including modified gravity theories, extra dimensions, rotating solutions, 2 + 1-dimensional spacetimes, and cylindrical configurations [49–63].

One of the most remarkable features of the Simpson–Visser solution is its ability to mimic the Schwarzschild

* marcos.sousa@uva.es

spacetime [13, 18, 64, 65]. Although it possesses a different photon ring structure, corresponding to unstable circular photon orbits, the shadow produced by the Simpson–Visser model is very similar to that of Schwarzschild, both in the case of a celestial sphere and in its optical appearance. Several works have explored the properties of this spacetime and its similarities with singular black hole solutions [66, 67]. Other black bounce models arising in different theoretical frameworks have also had their physical and observational properties extensively analyzed in the literature [68–70].

One of the most effective ways to analyze the physical properties of a black hole is through the behavior of matter and fields in its vicinity. A prominent example is the optical appearance of black holes [18, 19], which arises from both the distribution of surrounding matter, such as accretion disks, and the motion of photons emitted near the horizon. Another example is the dynamics of planets and stars orbiting supermassive black holes [71–74]. An important probe is provided by the tidal forces. Tidal forces arise from the inhomogeneity of the gravitational field, which generates a gradient of gravitational acceleration across an extended body [75]. This differential force produces a stretching effect and, if sufficiently strong, can overcome the internal binding forces of the object, leading to tidal disruption [76–78]. Such events commonly occur when astrophysical objects, such as stars, move in the vicinity of a black hole. The radius at which disruption takes place is known as the Roche limit or Roche radius [79, 80]. Since different black hole models generate different tidal force profiles, it is expected that their corresponding Roche limits may also be modified in a way that could, in principle, be observed astrophysically [81].

For the Schwarzschild black hole, the tidal forces diverge near the central singularity [75, 82]; however, this divergence is not observable because it is hidden behind the event horizon. In the Reissner–Nordström case, a particularly interesting phenomenon occurs: the tidal forces undergo a sign inversion, so that the body experiences compression instead of the usual stretching [81, 83, 84]. Not all black hole models exhibit divergent tidal forces; regular solutions such as the Bardeen black hole, among others, display finite tidal forces everywhere [81, 85–87]. In this way, tidal forces provide a powerful and insightful tool to investigate the behavior of matter in the vicinity of black holes and to discriminate between different theoretical models [88–90].

The structure of this paper is organized as follows. In Section II, we present the spacetime under consideration and discuss some of its main properties, as well as the radial geodesics in this geometry. In Section III, we derive the tidal forces for both a static observer and a radially infalling observer. In Section IV, we use the tidal forces to compute the Roche limit for this spacetime. Finally, the discussions, conclusions, and perspectives for future work are presented in Section V.

II. SPACETIME AND GEODESICS

Black bounces can be characterized as spacetimes in which the throat of a wormhole is hidden by the presence of horizons. The most well-known black bounce model is described by the Simpson–Visser spacetime, whose line element is usually written as [39]

$$ds^2 = -A(x)dt^2 + \frac{1}{A(x)}dx^2 + \Sigma(x)^2(d\theta^2 + \sin^2\theta d\phi^2),$$

$$A(x) = 1 - \frac{2M}{\Sigma(x)}, \quad \Sigma(x) = \sqrt{x^2 + a^2}. \quad (1)$$

This spacetime features a wormhole throat located at $x_t = 0$ and an event horizon located at $x_+ = \sqrt{4M^2 - a^2}$. It also possesses several other interesting properties. One example is the fact that, although the radius of the unstable photon orbit is given by $x_{ph} = \sqrt{9M^2 - a^2}$ for $a \leq 3M$, the radius of the apparent shadow of this spacetime is $x_S = 3\sqrt{3}M$ [6, 64, 91, 92], which coincides with the Schwarzschild result. Therefore, from the viewpoint of optical appearance and black hole shadow, the Simpson–Visser solution mimics the Schwarzschild black hole with remarkable efficiency [13, 18, 65].

Alternatively, by performing the coordinate transformation $r = \Sigma(x)$, we can rewrite the line element describing the Simpson–Visser spacetime as [56, 65, 86]

$$ds^2 = -A(r)dt^2 + \frac{1}{B(r)}dr^2 + r^2(d\theta^2 + \sin^2\theta d\phi^2),$$

$$A(r) = 1 - \frac{2M}{r}, \quad B(r) = \left(1 - \frac{2M}{r}\right)\left(1 - \frac{a^2}{r^2}\right). \quad (2)$$

In this coordinate system, the wormhole throat is located at $r_t = a$, while the event horizon radius is located at $r_+ = 2M$. It thus becomes clear that, if $a > 2M$, the throat radius exceeds the event horizon radius, so that the event horizon is no longer accessible and the spacetime describes a two-way traversable wormhole. In the case $a = 2M$, the horizon coincides with the wormhole throat, $r_t = r_+$, and the spacetime describes a one-way traversable wormhole. Thus, when the Simpson–Visser spacetime is written in terms of the coordinate r , we do not need to worry about the location of the event horizon radius for each value of a .

To study tidal forces in a given spacetime, it is crucial to analyze the geodesics followed by massive test particles in that spacetime. Associated with the line element (2), we have the Lagrangian

$$\mathcal{L} = \frac{1}{2}g_{\mu\nu}\dot{x}^\mu\dot{x}^\nu, \quad (3)$$

where the dot represents the derivative with respect to the proper time τ . For massive particles, we have $\mathcal{L} = -1/2$, and therefore

$$-1 = -At^2 + \frac{1}{2}\dot{r}^2 + r^2(\dot{\theta}^2 + \sin^2\theta\dot{\phi}^2). \quad (4)$$

For radial geodesics, we have $\dot{\theta} = \dot{\phi} = 0$, and thus the equation above can be simplified as

$$-1 = -\left(1 - \frac{2M}{r}\right) i^2 + \frac{\dot{r}^2}{\left(1 - \frac{2M}{r}\right)\left(1 - \frac{a^2}{r^2}\right)}. \quad (5)$$

From the Lagrangian (3), we can obtain the following conserved quantities

$$E = -\frac{\partial \mathcal{L}}{\partial \dot{t}} = A\dot{t}, \quad L = \frac{\partial \mathcal{L}}{\partial \dot{\phi}} = r^2 \sin^2 \theta \dot{\phi} = 0. \quad (6)$$

The constants L and E represent the angular momentum and the energy of the particle per unit mass, respectively. Using the constants of motion, we can write the following energy-balance equation

$$-1 = -\frac{E^2}{A} + \frac{\dot{r}^2}{B}. \quad (7)$$

From this relation, we can determine the energy of a particle released from rest at the radius $r = b$, which is given by

$$E = \sqrt{A(r = b)} = \sqrt{1 - \frac{2M}{b}}. \quad (8)$$

The particle energy will be important when we study the tidal forces in the case of a test body falling radially into the black hole.

III. TIDAL FORCES

In a curved spacetime, two nearby geodesics that are initially parallel may approach or separate. The relative acceleration between these geodesics is related to the tidal forces of the spacetime under consideration. This relative acceleration is described by the geodesic deviation equation, given by [82]

$$\frac{D^2 \xi^\mu}{D\tau^2} = K^\mu_{\gamma} \xi^\gamma, \quad (9)$$

where ξ^γ is the infinitesimal displacement vector between nearby geodesics and K^μ_{γ} is the tidal tensor given in by

$$K^\mu_{\gamma} = R^\mu_{\alpha\beta\gamma} v^\alpha v^\beta, \quad (10)$$

where $R^\mu_{\alpha\beta\gamma}$ is the Riemann tensor and v^α is the timelike vector tangent to the geodesic. The components of the tidal tensor provide information about the tidal forces exerted by a given compact object on a test body.

Since tensor components do not directly correspond to physically measured quantities and may contain coordinate artifacts, it is standard to project the components of the displacement vector and the tidal tensor onto an orthonormal tetrad adapted to the observer's four-velocity. This tetrad defines the observer's local inertial frame, providing a better physical interpretation. This

procedure yields coordinate-independent results, makes explicit the dependence of tidal forces on the observer's state of motion.

We consider a tetrad basis given by

$$\hat{e}^\mu_{\hat{a}} = (\hat{e}^\mu_{\hat{0}}, \hat{e}^\mu_{\hat{1}}, \hat{e}^\mu_{\hat{2}}, \hat{e}^\mu_{\hat{3}}), \quad (11)$$

where indices with hat denote tetrad indices. The chosen tetrad basis must satisfy the orthonormality condition

$$\hat{e}^\mu_{\hat{a}} \hat{e}^\nu_{\hat{b}} g_{\mu\nu} = \eta_{\hat{a}\hat{b}}. \quad (12)$$

The vector $\hat{e}^\mu_{\hat{0}}$ is the four-velocity of the observer and $\{\hat{e}^\mu_{\hat{1}}, \hat{e}^\mu_{\hat{2}}, \hat{e}^\mu_{\hat{3}}\}$ form an orthonormal basis for the spatial directions of the reference frame attached to the observer. Here, $\eta_{\hat{a}\hat{b}}$ represent the components of the Minkowski metric

In this formalism, the components of the tidal tensor are expressed with respect to the tetrad basis according to

$$K^{\hat{a}}_{\hat{b}} = e^{\hat{a}}_{\mu} e^{\nu}_{\hat{b}} K^\mu_{\nu}, \quad (13)$$

while the components of the displacement vector are

$$\xi^{\hat{a}} = e^{\hat{a}}_{\mu} \xi^\mu. \quad (14)$$

From this point on, we must choose an appropriate tetrad basis to describe the type of reference frame under consideration. Usually, three types of tetrad choices are employed: one associated with a static observer, another associated with a radially infalling observer, and finally one associated with an observer in circular motion. In this work, we focus on the first two cases.

A. Static Observer

We begin the study of tidal forces by considering the tetrad basis associated with a static observer. The tetrad basis corresponding to the line element (2) is given by [93]

$$\begin{aligned} \hat{e}^\mu_{\hat{0}} &= \left(\frac{1}{\sqrt{A}}, 0, 0, 0 \right), & \hat{e}^\mu_{\hat{1}} &= \left(0, \sqrt{B}, 0, 0 \right), \\ \hat{e}^\mu_{\hat{2}} &= \left(0, 0, \frac{1}{r}, 0 \right), & \hat{e}^\mu_{\hat{3}} &= \left(0, 0, 0, \frac{1}{r \sin \theta} \right). \end{aligned} \quad (15)$$

The tidal tensor associated with this tetrad basis is diagonal and can be written as

$$K^{\hat{a}}_{\hat{b}} = \text{diag}(0, K_1, K_2, K_3), \quad (16)$$

where

$$K_1 = -\frac{BA''}{2A} - \frac{A'B'}{4A} + \frac{BA'^2}{4A^2}, \quad (17)$$

$$K_2 = K_3 = -\frac{BA'}{2rA}. \quad (18)$$

For the Simpson–Visser spacetime, the components of the tidal force are given by

$$K_1 = \frac{M(2r^2 - 3a^2)}{r^5}, \quad K_2 = \frac{M(a^2 - r^2)}{r^5}. \quad (19)$$

It is straightforward to note that both the radial and angular components of the tidal forces vanish at

$$r_0^R = \sqrt{\frac{3}{2}}a, \quad \text{and} \quad r_0^A = a \quad (20)$$

respectively. This means that the angular component always vanishes at the wormhole throat. As for the radial component, depending on the value of a , the point at which $K_1 = 0$ can be located inside or outside the event horizon. More specifically, if $a > 2\sqrt{2/3}M$, the radial component vanishes outside the event horizon. Since $r \geq a$, we can see that the regularization parameter reduces the intensity of both the radial and angular components; thus, the larger the value of this parameter, the weaker the tidal forces. In the case of the angular component, there is no sign inversion of the force, so $K_2 = 0$ is the smallest allowed value to the intensity of the angular component. For the radial component, however, a sign inversion occurs and K_1 becomes negative in the interval $a \leq r < \sqrt{3/2}a$.

By solving conditions $dK_1/dr = 0$ and $dK_2/dr = 0$, we can obtain the extrema of the tidal forces. At these points, we can also compute the second derivative to determine whether the extrema correspond to maxima or minima. In this way, we find that these points are given by

$$r_{max}^R = \sqrt{\frac{5}{2}}a, \quad \text{and} \quad r_{min}^A = \sqrt{\frac{5}{3}}a. \quad (21)$$

Therefore, we find that the radial component attains a maximum value given by

$$K_1^{\max} = \frac{8\sqrt{2/5}M}{25a^3}, \quad (22)$$

which can be located outside the event horizon if $a > 2\sqrt{2/5}M$. On the other hand, the angular component attains a minimum value given by

$$K_2^{\min} = -\frac{6\sqrt{3/5}M}{25a^3}, \quad (23)$$

which can be located outside the event horizon if $a > 2\sqrt{3/5}M$.

In this way, the differences introduced by the Simpson–Visser spacetime with respect to the Schwarzschild spacetime can be observable outside the event horizon, depending on the value of the wormhole throat radius.

B. Radially infalling observer

We now study the tidal forces experienced by an observer falling radially into the black hole. For this configuration, the tetrad basis associated with such an observer

is given by [86]

$$\begin{aligned} \hat{e}_{\hat{0}}^{\mu} &= \left(\frac{E}{\sqrt{A}}, -\sqrt{\frac{B}{A}}\sqrt{E^2 - A}, 0, 0 \right), \\ \hat{e}_{\hat{1}}^{\mu} &= \left(-\frac{\sqrt{E^2 - A}}{A}, E\sqrt{\frac{B}{A}}, 0, 0 \right), \\ \hat{e}_{\hat{2}}^{\mu} &= \left(0, 0, \frac{1}{r}, 0 \right), \quad \hat{e}_{\hat{3}}^{\mu} = \left(0, 0, 0, \frac{1}{r\sin\theta} \right). \end{aligned} \quad (24)$$

The tidal tensor in this basis is given by

$$\bar{K}^{\hat{a}}_{\hat{b}} = \text{diag}(0, \bar{K}_1, \bar{K}_2, \bar{K}_3), \quad (25)$$

where

$$\bar{K}_1 = -\frac{BA''}{2A} - \frac{A'B'}{4A} + \frac{BA'^2}{4A^2}, \quad (26)$$

$$\bar{K}_2 = \bar{K}_3 = \frac{(E^2 - A)B'}{2rA} - \frac{E^2BA'}{2rA^2}. \quad (27)$$

It is interesting to note that, despite the more complicated tetrad basis, the radial component of the tidal force does not depend on the particle energy and remains the same as in the tetrad associated with a static observer, i.e. $\bar{K}_1 = K_1$. For the angular components, however, the situation is different: the angular component is more complicated and depends explicitly on the particle energy. Thus, depending on the choice of tetrad, at least some components of the tidal tensor are modified. It is also worth noting that, in spacetimes where $A = B$, the component \bar{K}_2 reduces to the same value obtained in the static case; therefore, in spacetimes such as Schwarzschild or Reissner–Nordström, this choice of tetrad does not modify the physical results.

Since $\bar{K}_1 = K_1$, we focus on the differences arising from \bar{K}_2 , which is given by

$$\bar{K}_2 = \frac{a^2((E^2 - 1)r + 3M) - Mr^2}{r^5}. \quad (28)$$

Once again, it becomes clear that there is a difference with respect to the static observer case, since the angular component of the tidal force now depends explicitly on the particle energy.

To assess the modifications induced by the presence of energy on the tidal forces, we first determine the point at which the angular component of the tidal force vanishes. This point is given by

$$\bar{r}_0^A = \frac{a^2(E^2 - 1) + a\sqrt{a^2(E^2 - 1)^2 + 12M^2}}{2M}. \quad (29)$$

In Figure 1, we compare the radius at which the angular component of the tidal force vanishes. We see that, even when the energy of a radially infalling test body tends to zero, this radius is still larger than the corresponding radius for the static observer. We also note that this radius increases as the energy increases. This allows,

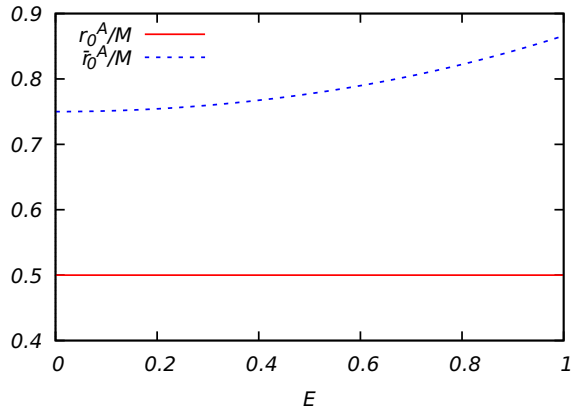


Figure 1. Comparison of the radius at which the angular component of the tidal force vanishes for both the static observer and the radially infalling observer as the energy is varied. In this case, we fix the throat radius to $a = 0.5M$.

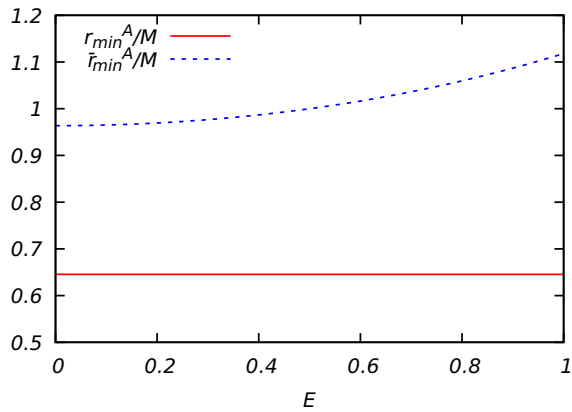


Figure 2. Comparison of the radius at which the angular component of the tidal force has its minimum value for both the static observer and the radially infalling observer as the energy is varied. In this case, we fix the throat radius to $a = 0.5M$.

unlike in the static observer case, for a sign inversion to occur in the angular component of the tidal force, and the larger the energy, the wider the interval over which this component becomes negative.

We now compute the point at which the angular component of the tidal force attains its minimum, obtaining

$$\bar{r}_{min}^A = \frac{2a^2(E^2 - 1) + \sqrt{4a^4(E^2 - 1)^2 + 45a^2M^2}}{3M}. \quad (30)$$

In Figure 2, we compare the radius at which the angular component of the tidal force reaches its minimum. We observe that, even when the energy of a radially infalling test body tends to zero, this radius remains larger than the corresponding radius for the static observer. We also note that this radius increases as the energy increases.

For the radially infalling case, the zero and the mini-

mum of the angular component, analogously to the static case, can occur outside the event horizon. In this configuration, the point at which the angular component vanishes is hidden inside the event horizon if

$$a < \frac{2M}{\sqrt{1 + 2E^2}}, \quad (31)$$

while the minimum point is hidden by the event horizon if

$$a < \frac{2\sqrt{3}M}{\sqrt{7 + 8E^2}}. \quad (32)$$

In this way, we see that the tidal forces in the Simpson–Visser spacetime differ from those in the Schwarzschild spacetime and, depending on the size of the wormhole throat, these differences can be located outside the event horizon and thus be observable.

In the next section, we will study how these modifications in the tidal forces affect the Roche limit for neutron stars, white dwarfs, and for Sun-like stars.

IV. TIDAL DISRUPTION IN THE SIMPSON–VISSEER SPACETIME

The Roche limit characterizes the critical distance at which an extended body held together solely by its own self-gravity can no longer withstand the tidal forces generated by an external gravitational field [76]. As an object approaches a sufficiently compact gravitational source, such as a dense star or a black hole, the spatial variation of the gravitational field across its finite size produces differential accelerations that tend to stretch the object along the radial direction and compress it along the transverse directions [75]. When these tidal forces exceed the internal gravitational binding (or other cohesive forces), the object undergoes tidal disruption, thereby defining the Roche limit [78].

In the context of relativistic compact objects, this concept must be formulated in terms of the tidal tensor. The Roche limit is determined by comparing the radial component of the tidal force with the internal binding force of the extended body because tidal disruption is driven primarily by radial stretching, so that, we can find the Roche radius, r_{Roche} , using [80]

$$\frac{1}{\xi^{\hat{1}}} \frac{D^2 \xi^{\hat{1}}}{D\tau^2} = K_1 = \frac{M_*}{R_*^3}, \quad (33)$$

where R_* and M_* denote the radius and mass of the star, respectively. We can rewrite the equation for the Roche limit as

$$\frac{M_* r^5}{R_*^3} - 2Mr^2 + 3Ma^2 = 0. \quad (34)$$

In this way, since the Roche radius depends on both the radius and the mass of the star subjected to an external

gravitational field, different stellar models exhibit distinct Roche limits. Consequently, it is necessary to explicitly specify the physical cases under consideration. In this work, we analyze three different stellar models: neutron stars, white dwarfs, and Sun-like stars.

Throughout this work, we adopt *natural units*, setting $c = G = 1$. Within this convention, the masses of black holes and stars acquire the same physical dimension as length. In contrast, in the International System of Units (SI), mass and length do not share the same unit of measurement. Therefore, astrophysical data must be appropriately converted into the unit system employed here in order to ensure a consistent comparison between physical quantities. In particular, a mass M expressed in SI units is mapped into a length scale according to $M \rightarrow \frac{GM}{c^2}$, which numerically yields $1 M_{\odot} \simeq 1.477$ km [94].

The mass and radius data for the stars considered in this work are listed in Table I.

Table I. Representative mass and radius values for the stellar models considered in this work [94] Masses are expressed in units of solar mass M_{\odot} , while radii are given in kilometers.

Stellar model	$M_{\star} [M_{\odot}]$	$M_{\star} [\text{km}]$	$R_{\star} [\text{km}]$
Neutron star	1.4	2.07	12
White dwarf	0.6	0.89	7.0×10^3
Sun-like star	1.0	1.48	6.96×10^5

For the Schwarzschild case, it is possible to solve Eq. (33) analytically. For the Simpson–Visser spacetime, however, this cannot be done analytically, and therefore we extract information about the Roche limit for this spacetime through graphical and numerical analysis.

A. Roche limit for neutron star

We now analyze the behavior of the Roche limit in the Simpson–Visser spacetime by considering a neutron star. Using the data in Table I, we take the star to have a mass of approximately $1.4 M_{\odot}$ and a radius of about 12 km. The results for the Roche radius are shown in Figure 3. In the left panel, we show how the Roche radius varies as the black hole mass is changed. We observe that the presence of the Simpson–Visser parameter imposes a maximum black hole mass for which a Roche radius exists. In this way, if the regularization parameter a is sufficiently large, the tidal forces are no longer able to overcome the binding forces, and the star does not undergo disruption. For those masses for which disruption still occurs for the values of a shown, we see that the Roche radius decreases as a increases, a behavior that is also confirmed in the right panel. Depending on the value of a , for a fixed black hole mass, the disruption may occur outside the event horizon, inside the horizon, or may not occur at all. For a black hole with mass $M = 9 M_{\odot}$, the Roche limit of a neutron star in the Schwarzschild case is $r_{\text{Roche}} = 28.11$ km, while the event horizon radius

is $r_+ = 26.64$ km; therefore, the disruption would take place outside the event horizon and would be observable. For the Simpson–Visser spacetime with parameter $a = 0.7M$, the Roche radius becomes $r_{\text{Roche}} = 26.21$ km, so that the disruption would occur only inside the horizon, whereas for $a = M$ the disruption would not occur at all.

For small values of a and sufficiently large black hole masses, the Roche radius becomes hidden inside the event horizon, as expected [95, 96]. Tidal forces evaluated near the event horizon decrease rapidly as the black hole mass increases, so that the disruption of neutron stars occurs inside the event horizon and is therefore not observable.

B. Roche limit for white dwarf

As discussed in the previous subsection, for masses $M \approx 10 M_{\odot}$ neutron stars undergo disruption only when it is hidden by the event horizon, if disruption occurs at all, even for small values of a . We now use Eq. (34), together with the data from Table I, to verify whether this behavior also occurs for a white dwarf.

In Figure 4, we analyze the behavior of the Roche radius for white dwarfs. In the left panel, we show how the Roche radius varies as the black hole mass is increased for selected values of the regularization parameter, and we observe that the larger the regularization parameter, the smaller the black hole mass for which the Roche radius exists. In the right panel, we fix the black hole mass and study how the Roche radius behaves as the regularization parameter is varied, finding the same trend: more massive black holes allow only smaller values of the regularization parameter.

For those cases in which the combination of black hole mass and regularization parameter permits disruption, more massive black holes have the Roche radius hidden inside the event horizon. For astrophysical black holes such as M87*, with mass $M = 6.5 \times 10^9 M_{\odot}$ [2], and Sgr A*, with mass $M = 4.297 \times 10^6 M_{\odot}$ [1], white dwarfs would have a Roche radius smaller than the event horizon radius, and thus the disruption process would be hidden by the event horizon. For the case of M87*, a Roche radius exists only if the regularization parameter satisfies approximately $a \lesssim 9.4 \times 10^{-4} M$. In this situation, the Roche radius is $r_{\text{Roche}} \approx 1.5 \times 10^7$ km, while the event horizon radius is $r_+ \approx 1.92 \times 10^{10}$ km; therefore, the horizon radius is much larger than the Roche radius. For Sgr A*, a Roche limit exists provided that the regularization parameter satisfies approximately $a \lesssim 1.2 \times 10^{-1} M$. In this case, the Roche radius is $r_{\text{Roche}} \approx 1.39 \times 10^6$ km, whereas the event horizon radius is $r_+ \approx 1.27 \times 10^7$ km. Although the difference is smaller in this case, the Roche radius still remains smaller than the event horizon radius.

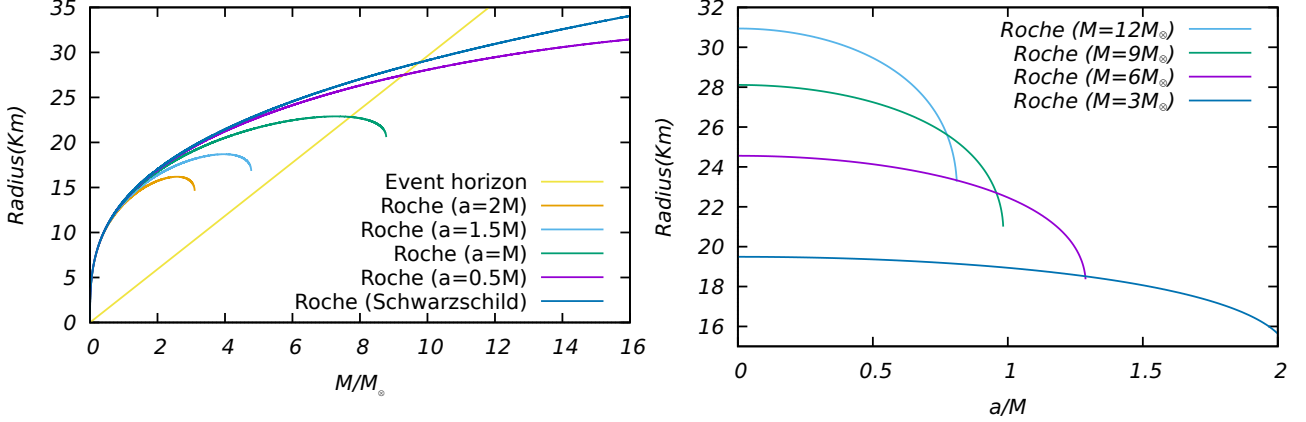


Figure 3. In the left panel, we compare the Roche radius of a neutron star for different values of a with the event horizon radius as the black hole mass is varied. In the right panel, we show how the Roche radius behaves as the parameter a is varied for different values of the black hole mass.

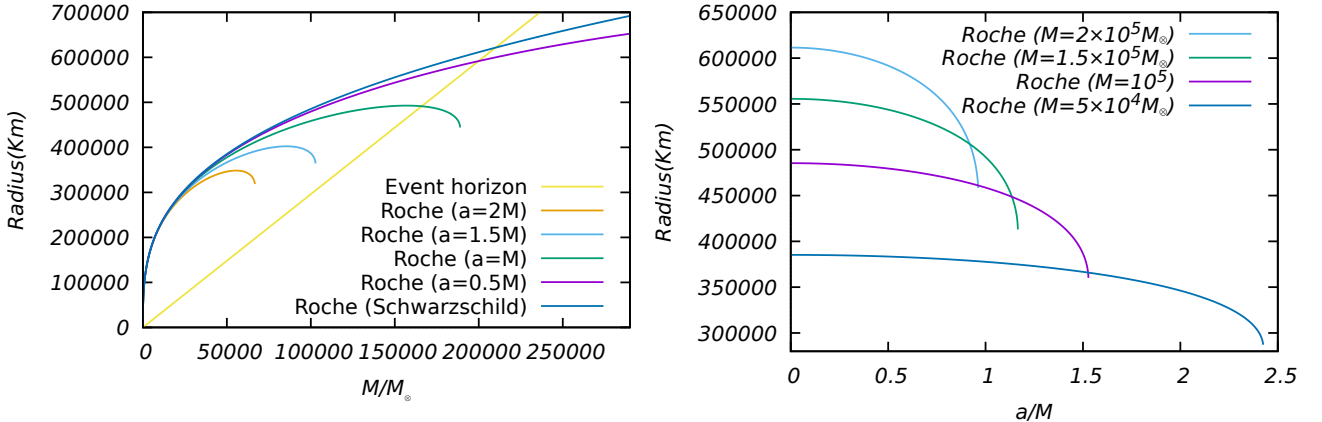


Figure 4. In the left panel, we compare the Roche radius of a white dwarf for different values of a with the event horizon radius as the black hole mass is varied. In the right panel, we show how the Roche radius behaves as the parameter a is varied for different values of the black hole mass.

C. Roche limit for Sun-like star

As a final case, we now analyze the Roche limit for Sun-like stars and investigate whether the disruption process for this stellar model differs from the two previous cases.

In Figure 5, we analyze the behavior of the Roche radius for Sun-like stars. In the left panel, we show how the Roche radius varies as the black hole mass is increased for selected values of the regularization parameter, and we observe that the larger the regularization parameter, the smaller the black hole mass for which the Roche radius exists. In the right panel, we fix the black hole mass and study how the Roche radius behaves as the regularization parameter is varied, finding the same trend: more massive black holes allow only smaller values of the regularization parameter.

For those cases in which the combination of black hole mass and regularization parameter permits disruption, more massive black holes have the Roche radius hidden

inside the event horizon. For astrophysical black holes such as M87*, with mass $M = 6.5 \times 10^9 M_\odot$, Sun-like stars would have a Roche radius smaller than the event horizon radius, and thus the disruption process would be hidden by the event horizon. For the case in which the black hole is as massive as M87*, a Roche limit exists only if the regularization parameter satisfies approximately $a \lesssim 7.93 \times 10^{-2} M$. In this situation, the Roche radius is $r_{\text{Roche}} \approx 1.21 \times 10^9$ km, while the event horizon radius is $r_+ \approx 1.92 \times 10^{10}$ km. Although the difference is much smaller than in the white-dwarf case, the disruption process would still be hidden inside the event horizon.

However, for the case of Sgr A*, with mass $M = 4.297 \times 10^6 M_\odot$, the black hole mass is small enough that the Roche radius, for the values of a considered, is larger than the event horizon radius. In this way, even in the case of a supermassive black hole such as Sgr A*, the disruption process can be observable, allowing us to probe astrophysically how the Simpson–Visser regular-

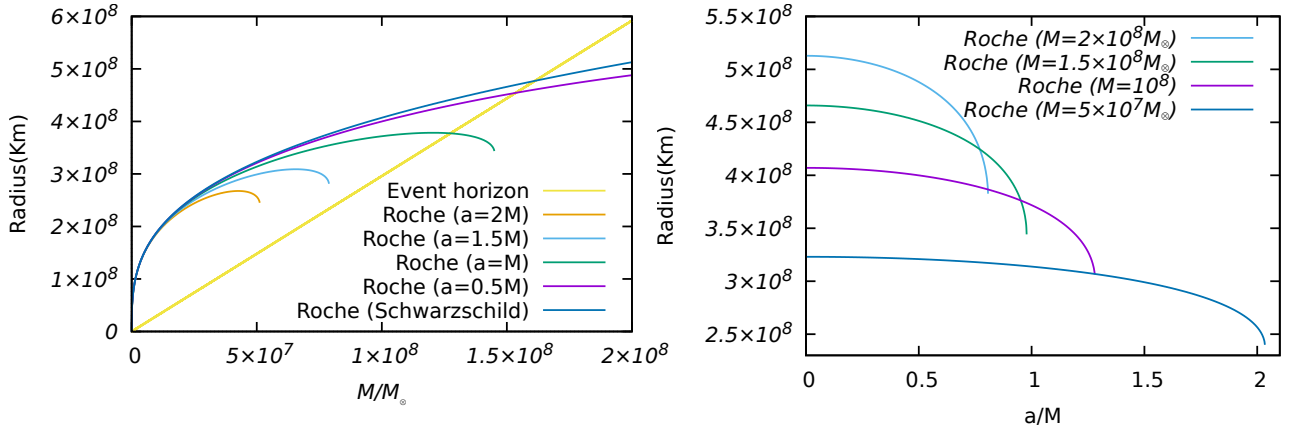


Figure 5. In the left panel, we compare the Roche radius of a Sun-like star for different values of a with the event horizon radius as the black hole mass is varied. In the right panel, we show how the Roche radius behaves as the parameter a is varied for different values of the black hole mass.

ization may influence the spacetime around the black hole. For black holes as massive as Sgr A*, a Roche limit exists if the regularization parameter satisfies approximately $a \lesssim 10.45M$, a value that is well above the upper bound for which an event horizon is still present. As an illustrative example within the horizon regime, we may consider $a = M$, for which the Roche radius is $r_{\text{Roche}} \approx 1.42 \times 10^8$ km, while the event horizon radius is $r_+ \approx 1.27 \times 10^7$ km. In this case, the stellar disruption would occur outside the event horizon and would therefore be observable.

V. SUMMARY AND CONCLUSION

In this work, we studied the tidal forces and the Roche limit for a black bounce spacetime described by the Simpson–Visser metric. This spacetime possesses several remarkable features, such as the presence of a wormhole throat hidden behind an event horizon, as well as its ability to mimic with high efficiency some characteristics of the Schwarzschild black hole.

In Section II, we present the spacetime under consideration and discuss some of its main properties, such as the fact that event horizons exist only if $a \leq 2M$, whereas for $a > 2M$ the solution describes a two-way traversable wormhole. We also discuss that, depending on the coordinate system adopted, the radius of the unstable photon orbit differs from the Schwarzschild case, while the radius of the black hole shadow remains the same in both cases, provided that $a \leq 3M$. In addition, we present the radial geodesics, which are essential to determine the energy of a particle depending on the position from which it is released.

In Section III, we derived the tidal forces for the Simpson–Visser spacetime. We developed the formalism to study tidal forces through the analysis of the components of the tidal tensor appearing in the geodesic de-

viation equation. However, obtaining the tidal-tensor components alone is not sufficient to analyze tidal effects; it is also necessary to choose an appropriate local frame that characterizes the type of observer. We first considered the case of a static observer by selecting a suitable tetrad basis and projecting the tidal tensor onto this frame. We found that the tidal forces in this case do not diverge, since $r = 0$ does not belong to the manifold and the radial coordinate is restricted to the interval $[a, \infty)$. We obtained that the angular component vanishes at the wormhole throat, $r = a$, while the radial component vanishes at $r = \sqrt{3/2}a$. The radial component attains a maximum value $K_1^{\max} = \frac{8\sqrt{2/5}M}{25a^3}$ at $r = \sqrt{5/2}a$, whereas the angular component attains a minimum value $K_2^{\min} = -\frac{6\sqrt{3/5}M}{25a^3}$ at $r = \sqrt{5/3}a$. We also studied the case of a radially infalling observer and found that the radial component of the tidal force coincides with the static case. In contrast, the angular component is modified and now depends explicitly on the energy. The radii at which the angular component vanishes or reaches its minimum are larger than in the static case and increase as the energy increases, as shown in Figures 1 and 2.

In Section IV, we used the radial component of the tidal forces to determine the Roche limit for three types of stars: neutron stars, white dwarfs, and Sun-like stars. For neutron stars, which are highly compact and therefore have a large mass concentrated within a relatively small radius, the Roche radius is typically smaller than the black hole horizon radius when the black hole mass is of the order of $10M_\odot$. Moreover, the regularization parameter further reduces the Roche radius. As a consequence, the Roche limit may be observable in the Schwarzschild case but not in the Simpson–Visser spacetime, depending on the value of the regularization parameter. For a fixed black hole mass, if a is sufficiently large, no real solution for the Roche radius exists, implying

that the star does not undergo tidal disruption. Only for relatively small black hole masses and sufficiently small values of a can the Roche limit be located outside the event horizon. Black holes in this mass range may be observed astrophysically in coalescence events accompanied by gravitational-wave emission [97].

For white dwarfs, which are less compact than neutron stars, the Roche limit can be observable outside the event horizon over a much wider mass range. However, for supermassive black holes such as Sgr A* and M87*, this limit is not observable, since the Roche radius is smaller than the event horizon radius. As in the previous case, for a fixed mass there exists a maximum value of a beyond which the Roche radius ceases to exist, implying the absence of tidal disruption. For Sgr A* and M87*, these critical values of a are of the order of $10^{-1}M$ and $10^{-4}M$, respectively.

Finally, we analyzed the Roche limit for Sun-like stars and found that supermassive black holes such as Sgr A* possess an observable Roche limit, since in this case the Roche radius exceeds the event horizon radius. This allows tidal disruption to occur even for relatively large values of the regularization parameter, well above the bound required for the existence of an event horizon. For black holes with masses comparable to that of M87*, however,

the Roche radius becomes hidden inside the event horizon, making stellar disruption unobservable, and the regularization parameter must be restricted to values of order $10^{-2}M$ for disruption to occur.

In general, in all cases the regularization parameter decreases the Roche radius as a increases, until a point is reached at which no real Roche radius exists and tidal disruption no longer occurs.

In future work, we plan to investigate whether this behavior of the Roche limit persists for other black bounce models. We also intend to study the rotating case in order to determine how rotation influences the tidal forces and the Roche limit, since astrophysical black holes are not static.

ACKNOWLEDGEMENTS

M.S. thanks Conselho Nacional de Desenvolvimento Científico e Tecnológico - CNPq, Brazil, CNPQ/PDE 200218/2025-5, for financial support. The paper is also supported by the Spanish project PID2024-157196NB-I00 funded by MICIU/AEI/10.13039/501100011033.

- [1] Kazunori Akiyama *et al.* (Event Horizon Telescope), “First Sagittarius A* Event Horizon Telescope Results. I. The Shadow of the Supermassive Black Hole in the Center of the Milky Way,” *Astrophys. J. Lett.* **930**, L12 (2022), arXiv:2311.08680 [astro-ph.HE].
- [2] Kazunori Akiyama *et al.* (Event Horizon Telescope), “First M87 Event Horizon Telescope Results. I. The Shadow of the Supermassive Black Hole,” *Astrophys. J. Lett.* **875**, L1 (2019), arXiv:1906.11238 [astro-ph.GA].
- [3] Kazunori Akiyama *et al.* (Event Horizon Telescope), “First Sagittarius A* Event Horizon Telescope Results. II. EHT and Multiwavelength Observations, Data Processing, and Calibration,” *Astrophys. J. Lett.* **930**, L13 (2022), arXiv:2311.08679 [astro-ph.HE].
- [4] Kazunori Akiyama *et al.* (Event Horizon Telescope), “First M87 Event Horizon Telescope Results. II. Array and Instrumentation,” *Astrophys. J. Lett.* **875**, L2 (2019), arXiv:1906.11239 [astro-ph.IM].
- [5] Kazunori Akiyama *et al.* (Event Horizon Telescope), “First M87 Event Horizon Telescope Results. III. Data Processing and Calibration,” *Astrophys. J. Lett.* **875**, L3 (2019), arXiv:1906.11240 [astro-ph.GA].
- [6] Sunny Vagnozzi *et al.*, “Horizon-scale tests of gravity theories and fundamental physics from the Event Horizon Telescope image of Sagittarius A,” *Class. Quant. Grav.* **40**, 165007 (2023), arXiv:2205.07787 [gr-qc].
- [7] Leor Barack *et al.*, “Black holes, gravitational waves and fundamental physics: a roadmap,” *Class. Quant. Grav.* **36**, 143001 (2019), arXiv:1806.05195 [gr-qc].
- [8] Vitor Cardoso and Paolo Pani, “Tests for the existence of black holes through gravitational wave echoes,” *Nature Astron.* **1**, 586–591 (2017), arXiv:1709.01525 [gr-qc].
- [9] K. G. Arun *et al.* (LISA), “New horizons for fundamental physics with LISA,” *Living Rev. Rel.* **25**, 4 (2022), arXiv:2205.01597 [gr-qc].
- [10] Pedro V. P. Cunha and Carlos A. R. Herdeiro, “Shadows and strong gravitational lensing: a brief review,” *Gen. Rel. Grav.* **50**, 42 (2018), arXiv:1801.00860 [gr-qc].
- [11] Carlos A. R. Herdeiro, Alexandre M. Pombo, Eugen Radu, Pedro V. P. Cunha, and Nicolas Sanchis-Gual, “The imitation game: Proca stars that can mimic the Schwarzschild shadow,” *JCAP* **04**, 051 (2021), arXiv:2102.01703 [gr-qc].
- [12] Ivo Sengo, Pedro V. P. Cunha, Carlos A. R. Herdeiro, and Eugen Radu, “The imitation game reloaded: effective shadows of dynamically robust spinning Proca stars,” *JCAP* **05**, 054 (2024), arXiv:2402.14919 [gr-qc].
- [13] Haroldo C. D. Lima, Junior., Luís C. B. Crispino, Pedro V. P. Cunha, and Carlos A. R. Herdeiro, “Can different black holes cast the same shadow?” *Phys. Rev. D* **103**, 084040 (2021), arXiv:2102.07034 [gr-qc].
- [14] Vitor Cardoso, Edgardo Franzin, and Paolo Pani, “Is the gravitational-wave ringdown a probe of the event horizon?” *Phys. Rev. Lett.* **116**, 171101 (2016), [Erratum: *Phys. Rev. Lett.* 117, 089902 (2016)], arXiv:1602.07309 [gr-qc].
- [15] Pedro V. P. Cunha, Carlos A. R. Herdeiro, and Maria J. Rodriguez, “Does the black hole shadow probe the event horizon geometry?” *Phys. Rev. D* **97**, 084020 (2018), arXiv:1802.02675 [gr-qc].
- [16] João Luís Rosa, Daniela S. J. Cordeiro, Caio F. B. Macedo, and Francisco S. N. Lobo, “Observational imprints of gravastars from accretion disks and hot spots,” *Phys. Rev. D* **109**, 084002 (2024), arXiv:2401.07766 [gr-qc].

qc].

[17] João Luís Rosa, Caio F. B. Macedo, and Diego Rubiera-Garcia, “Imaging compact boson stars with hot spots and thin accretion disks,” *Phys. Rev. D* **108**, 044021 (2023), [arXiv:2303.17296 \[gr-qc\]](#).

[18] Merce Guerrero, Gonzalo J. Olmo, Diego Rubiera-Garcia, and Diego Sáez-Chillón Gómez, “Shadows and optical appearance of black bounces illuminated by a thin accretion disk,” *JCAP* **08**, 036 (2021), [arXiv:2105.15073 \[gr-qc\]](#).

[19] Merce Guerrero, Gonzalo J. Olmo, Diego Rubiera-Garcia, and Diego Gómez Sáez-Chillón, “Light ring images of double photon spheres in black hole and wormhole spacetimes,” *Phys. Rev. D* **105**, 084057 (2022), [arXiv:2202.03809 \[gr-qc\]](#).

[20] Stefano Ansoldi, “Spherical black holes with regular center: A Review of existing models including a recent realization with Gaussian sources,” in *Conference on Black Holes and Naked Singularities* (2008) [arXiv:0802.0330 \[gr-qc\]](#).

[21] Kirill A. Bronnikov, “Regular magnetic black holes and monopoles from nonlinear electrodynamics,” *Phys. Rev. D* **63**, 044005 (2001), [arXiv:gr-qc/0006014](#).

[22] K. A. Bronnikov and J. C. Fabris, “Regular phantom black holes,” *Phys. Rev. Lett.* **96**, 251101 (2006), [arXiv:gr-qc/0511109](#).

[23] Kirill A. Bronnikov, “Regular black holes sourced by nonlinear electrodynamics,” (2022), [arXiv:2211.00743 \[gr-qc\]](#).

[24] Sean A. Hayward, “Formation and evaporation of regular black holes,” *Phys. Rev. Lett.* **96**, 031103 (2006), [arXiv:gr-qc/0506126](#).

[25] R. A. Konoplya and A. Zhidenko, “Dark matter halo as a source of regular black-hole geometries,” (2025), [arXiv:2511.03066 \[gr-qc\]](#).

[26] Eloy Ayon-Beato and Alberto Garcia, “The Bardeen model as a nonlinear magnetic monopole,” *Phys. Lett. B* **493**, 149–152 (2000), [arXiv:gr-qc/0009077](#).

[27] Manuel E. Rodrigues and Marcos V. de Sousa Silva, “Bardeen Regular Black Hole With an Electric Source,” *JCAP* **06**, 025 (2018), [arXiv:1802.05095 \[gr-qc\]](#).

[28] Manuel E. Rodrigues, Ednaldo L. B. Junior, and Marcos V. de Sousa Silva, “Using dominant and weak energy conditions for build new classe of regular black holes,” *JCAP* **02**, 059 (2018), [arXiv:1705.05744 \[physics.gen-ph\]](#).

[29] Eloy Ayon-Beato and Alberto Garcia, “Regular black hole in general relativity coupled to nonlinear electrodynamics,” *Phys. Rev. Lett.* **80**, 5056–5059 (1998), [arXiv:gr-qc/9911046](#).

[30] Eloy Ayon-Beato and Alberto Garcia, “New regular black hole solution from nonlinear electrodynamics,” *Phys. Lett. B* **464**, 25 (1999), [arXiv:hep-th/9911174](#).

[31] Irina Dymnikova, “Regular electrically charged structures in nonlinear electrodynamics coupled to general relativity,” *Class. Quant. Grav.* **21**, 4417–4429 (2004), [arXiv:gr-qc/0407072](#).

[32] Leonardo Balart and Elias C. Vagenas, “Regular black holes with a nonlinear electrodynamics source,” *Phys. Rev. D* **90**, 124045 (2014), [arXiv:1408.0306 \[gr-qc\]](#).

[33] Ednaldo L. B. Junior, Manuel E. Rodrigues, and Marcos V. de Sousa Silva, “Regular black holes in Rainbow Gravity,” *Nucl. Phys. B* **961**, 115244 (2020), [arXiv:2002.04410 \[gr-qc\]](#).

[34] Manuel E. Rodrigues and Marcos V. de Sousa Silva, “Regular multihorizon black holes in $f(G)$ gravity with nonlinear electrodynamics,” *Phys. Rev. D* **99**, 124010 (2019), [arXiv:1906.06168 \[gr-qc\]](#).

[35] Manuel E. Rodrigues, Marcos V. de S. Silva, and Henrique A. Vieira, “Bardeen-Kiselev black hole with a cosmological constant,” *Phys. Rev. D* **105**, 084043 (2022), [arXiv:2203.04965 \[gr-qc\]](#).

[36] Manuel E. Rodrigues, Marcos V. de Sousa Silva, and Andrew S. de Siqueira, “Regular multihorizon black holes in General Relativity,” *Phys. Rev. D* **102**, 084038 (2020), [arXiv:2010.09490 \[gr-qc\]](#).

[37] Marcos V. de Sousa Silva and Manuel E. Rodrigues, “Regular black holes in $f(G)$ gravity,” *Eur. Phys. J. C* **78**, 638 (2018), [arXiv:1808.05861 \[gr-qc\]](#).

[38] Matt Visser and David Hochberg, “Generic wormhole throats,” *Annals Israel Phys. Soc.* **13**, 249 (1997), [arXiv:gr-qc/9710001](#).

[39] Alex Simpson and Matt Visser, “Black-bounce to traversable wormhole,” *JCAP* **02**, 042 (2019), [arXiv:1812.07114 \[gr-qc\]](#).

[40] Edgardo Franzin, Stefano Liberati, Jacopo Mazza, Alex Simpson, and Matt Visser, “Charged black-bounce spacetimes,” *JCAP* **07**, 036 (2021), [arXiv:2104.11376 \[gr-qc\]](#).

[41] Francisco S. N. Lobo, Manuel E. Rodrigues, Marcos V. de Sousa Silva, Alex Simpson, and Matt Visser, “Novel black-bounce spacetimes: wormholes, regularity, energy conditions, and causal structure,” *Phys. Rev. D* **103**, 084052 (2021), [arXiv:2009.12057 \[gr-qc\]](#).

[42] Pedro Cañate, “Black bounces as magnetically charged phantom regular black holes in Einstein-nonlinear electrodynamics gravity coupled to a self-interacting scalar field,” *Phys. Rev. D* **106**, 024031 (2022), [arXiv:2202.02303 \[gr-qc\]](#).

[43] Kirill A. Bronnikov and Rahul Kumar Walia, “Field sources for Simpson-Visser spacetimes,” *Phys. Rev. D* **105**, 044039 (2022), [arXiv:2112.13198 \[gr-qc\]](#).

[44] Manuel E. Rodrigues and Marcos V. de S. Silva, “Source of black bounces in general relativity,” *Phys. Rev. D* **107**, 044064 (2023), [arXiv:2302.10772 \[gr-qc\]](#).

[45] Daniela S. J. Cordeiro, Ednaldo L. B. Junior, José Tarçiso S. S. Junior, Francisco S. N. Lobo, Jorde A. A. Ramos, Manuel E. Rodrigues, Luís F. Dias da Silva, and Henrique A. Vieira, “Black bounce solutions via nonminimal scalar-electrodynamical couplings,” (2025), [arXiv:2509.24053 \[gr-qc\]](#).

[46] Júlio C. Fabris, Ednaldo L. B. Junior, and Manuel E. Rodrigues, “Generalized models for black-bounce solutions in $f(R)$ gravity,” *Eur. Phys. J. C* **83**, 884 (2023), [arXiv:2310.00714 \[gr-qc\]](#).

[47] Manuel E. Rodrigues and Marcos V. de S. Silva, “Comment on ‘Source of black bounces in Rastall gravity’,” *JCAP* **05**, 012 (2024), [arXiv:2402.17814 \[gr-qc\]](#).

[48] Marcos V. de S. Silva, T. M. Crispim, G. Alencar, R. R. Landim, and Manuel E. Rodrigues, “Generalized black-bounces solutions in $f(R)$ gravity and their field sources,” *Class. Quant. Grav.* **43**, 015005 (2026), [arXiv:2502.19186 \[gr-qc\]](#).

[49] Manuel E. Rodrigues and Marcos V. de S. Silva, “Black-bounces with multiple throats and anti-throats,” *Class. Quant. Grav.* **40**, 225011 (2023), [arXiv:2204.11851 \[gr-qc\]](#).

[50] Manuel E. Rodrigues and Marcos V. de S. Silva, “Embedding regular black holes and black bounces in a cloud of strings,” *Phys. Rev. D* **106**, 084016 (2022), [arXiv:2210.05383 \[gr-qc\]](#).

[51] Kirill A. Bronnikov, Manuel E. Rodrigues, and Marcos V. de S. Silva, “Cylindrical black bounces and their field sources,” *Phys. Rev. D* **108**, 024065 (2023), [arXiv:2305.19296 \[gr-qc\]](#).

[52] G. Alencar, Kirill A. Bronnikov, Manuel E. Rodrigues, Diego Sáez-Chillón Gómez, and Marcos V. de S. Silva, “On black bounce space-times in nonlinear electrodynamics,” *Eur. Phys. J. C* **84**, 745 (2024), [arXiv:2403.12897 \[gr-qc\]](#).

[53] Carlos F. S. Pereira, Denis C. Rodrigues, Marcos V. de S. Silva, Júlio C. Fabris, Manuel E. Rodrigues, and H. Belich, “Magnetically charged black-bounce solution via nonlinear electrodynamics in a k-essence theory,” *Phys. Rev. D* **111**, 084025 (2025), [arXiv:2409.09182 \[gr-qc\]](#).

[54] G. Alencar, M. Nilton, Manuel E. Rodrigues, and Marcos V. de S. Silva, “Field sources for $f(R, R\mu\nu)$ black-bounce solutions: The case of K-gravity,” *Phys. Dark Univ.* **49**, 102060 (2025), [arXiv:2409.12101 \[gr-qc\]](#).

[55] Carlos F. S. Pereira, Marcos V. de S. Silva, H. Belich, Denis C. Rodrigues, Júlio C. Fabris, and Manuel E. Rodrigues, “Black-bounce solutions in a k-essence theory under the effects of bumblebee gravity,” *Phys. Rev. D* **111**, 124005 (2025), [arXiv:2503.09920 \[gr-qc\]](#).

[56] Marcos V. de S. Silva, Carlos F. S. Pereira, G. Alencar, and Celio R. Muniz, “Lqq inspired spacetimes as solutions of the Einstein equations,” *Gen. Rel. Grav.* **57**, 168 (2025), [arXiv:2506.19818 \[gr-qc\]](#).

[57] G. Alencar, Albert Duran-Cabacés, Diego Rubiera-Garcia, and Diego Sáez-Chillón Gómez, “General spherically symmetric black bounces within nonlinear electrodynamics,” *Phys. Rev. D* **111**, 104020 (2025), [arXiv:2501.03909 \[gr-qc\]](#).

[58] C. R. Muniz, G. Alencar, M. S. Cunha, and Gonzalo J. Olmo, “Static and stationary black bounces inspired by loop quantum gravity,” *Phys. Rev. D* **112**, 024018 (2025), [arXiv:2408.08542 \[gr-qc\]](#).

[59] T. M. Crispim, G. Alencar, and Milko Estrada, “Braneworld Black Bounce to Transversable Wormhole Analytically Connected to an asymptotically AdS_5 Boundary,” (2024), [arXiv:2407.03528 \[gr-qc\]](#).

[60] Tiago M. Crispim, Milko Estrada, C. R. Muniz, and G. Alencar, “Braneworld black bounce to transversable wormhole,” *JCAP* **10**, 063 (2024), [arXiv:2405.08048 \[hep-th\]](#).

[61] Arthur Menezes Lima, Geová Maciel de Alencar Filho, and Job Saraiva Furtado Neto, “Black String Bounce to Traversable Wormhole,” *Symmetry* **15**, 150 (2023), [arXiv:2211.12349 \[gr-qc\]](#).

[62] A. Lima, G. Alencar, R. N. Costa Filho, and R. R. Landim, “Charged black string bounce and its field source,” *Gen. Rel. Grav.* **55**, 108 (2023), [arXiv:2306.03029 \[gr-qc\]](#).

[63] Ednaldo L. B. Junior, José Tarciso S. S. Junior, Francisco S. N. Lobo, Manuel E. Rodrigues, Diego Rubiera-Garcia, Luís F. Dias da Silva, and Henrique A. Vieira, “Black bounces in Cotton gravity,” *Eur. Phys. J. C* **84**, 1190 (2024), [arXiv:2407.21649 \[gr-qc\]](#).

[64] Marcos V. de S. Silva and Manuel E. Rodrigues, “Orbits Around a Black Bounce Spacetime,” *Int. J. Theor. Phys.* **63**, 101 (2024), [arXiv:2404.15792 \[gr-qc\]](#).

[65] Edgardo Franzin, Stefano Liberati, and Vania Vellucci, “From regular black holes to horizonless objects: quasinormal modes, instabilities and spectroscopy,” *JCAP* **01**, 020 (2024), [arXiv:2310.11990 \[gr-qc\]](#).

[66] C. F. S. Pereira, A. R. Soares, M. V. de S. Silva, R. L. L. Vitória, and H. Belich, “Light deflection and gravitational lensing effects in acoustic black-bounce spacetime,” *Phys. Rev. D* **112**, 064012 (2025), [arXiv:2505.12577 \[gr-qc\]](#).

[67] J. R. Nascimento, A. Yu. Petrov, P. J. Porfirio, and A. R. Soares, “Gravitational lensing in black-bounce spacetimes,” *Phys. Rev. D* **102**, 044021 (2020), [arXiv:2005.13096 \[gr-qc\]](#).

[68] A. R. Soares, C. F. S. Pereira, R. L. L. Vitória, Marcos V. de S. Silva, and H. Belich, “Light deflection and gravitational lensing effects inspired by loop quantum gravity,” *JCAP* **06**, 034 (2025), [arXiv:2503.06373 \[gr-qc\]](#).

[69] A. R. Soares, R. L. L. Vitória, and C. F. S. Pereira, “Topologically charged holonomy corrected Schwarzschild black hole lensing,” *Phys. Rev. D* **110**, 084004 (2024), [arXiv:2408.03217 \[gr-qc\]](#).

[70] A. R. Soares, C. F. S. Pereira, R. L. L. Vitória, and Erick Melo Rocha, “Holonomy corrected Schwarzschild black hole lensing,” *Phys. Rev. D* **108**, 124024 (2023), [arXiv:2309.05106 \[gr-qc\]](#).

[71] R. Abuter *et al.* (GRAVITY), “Detection of the gravitational redshift in the orbit of the star S2 near the Galactic centre massive black hole,” *Astron. Astrophys.* **615**, L15 (2018), [arXiv:1807.09409 \[astro-ph.GA\]](#).

[72] R. Abuter *et al.* (GRAVITY), “Detection of the Schwarzschild precession in the orbit of the star S2 near the Galactic centre massive black hole,” *Astron. Astrophys.* **636**, L5 (2020), [arXiv:2004.07187 \[astro-ph.GA\]](#).

[73] Reinhard Genzel, Frank Eisenhauer, and Stefan Gillessen, “The Galactic Center Massive Black Hole and Nuclear Star Cluster,” *Rev. Mod. Phys.* **82**, 3121–3195 (2010), [arXiv:1006.0064 \[astro-ph.GA\]](#).

[74] W. Ishibashi, “How black hole activity may influence exoplanetary evolution in our Galaxy,” *Mon. Not. Roy. Astron. Soc.* **533**, 455 (2024), [arXiv:2410.22428 \[astro-ph.GA\]](#).

[75] M. P. Hobson, G. P. Efstathiou, and A. N. Lasenby, *General relativity: An introduction for physicists* (Cambridge University Press, 2006).

[76] Sudi Gezari, “Tidal Disruption Events,” *Ann. Rev. Astron. Astrophys.* **59**, 21–58 (2021), [arXiv:2104.14580 \[astro-ph.HE\]](#).

[77] Ashok B. Joshi, Pankaj S. Joshi, and Sudip Bhattacharyya, “Tidal disruption of a neutron star near naked singularity,” (2025), [arXiv:2509.26108 \[gr-qc\]](#).

[78] S. Komossa, “Tidal disruption of stars by supermassive black holes: Status of observations,” *JHEAp* **7**, 148–157 (2015), [arXiv:1505.01093 \[astro-ph.HE\]](#).

[79] Charles R. Evans and Christopher S. Kochanek, “The tidal disruption of a star by a massive black hole,” *Astrophys. J. Lett.* **346**, L13–L16 (1989).

[80] Ednaldo L. B. Junior, Herlan N. Lemos, and Marcos V. de S. Silva, “Tidal dynamics and stellar disruption in charged Kalb-Ramond black holes in nonlinear electrodynamics,” (2026), [arXiv:2601.09482 \[gr-qc\]](#).

[81] Haroldo C. D. Lima Junior, Mateus M. Corrêa, Caio F. B. Macedo, and Luís C. B. Crispino, “Tidal forces in dirty black hole spacetimes,” *Eur. Phys. J. C* **82**, 479 (2022), [arXiv:2205.13569 \[gr-qc\]](#).

[82] R. d’Inverno and J. Vickers, *Introducing Einstein’s Relativity: A Deeper Understanding* (Oxford University Press, 2022).

[83] Luís C. B. Crispino, Atsushi Higuchi, Leandro A. Oliveira, and Ednilton S. de Oliveira, “Tidal forces in Reissner–Nordström spacetimes,” *Eur. Phys. J. C* **76**, 168 (2016), arXiv:1602.07232 [gr-qc].

[84] M. Sharif and Lubna Kousar, “Tidal Forces in Dyonic Reissner–Nördstrom Black Hole,” *Commun. Theor. Phys.* **69**, 257 (2018).

[85] Haroldo C. D. Lima and Luís C. B. Crispino, “Tidal forces in the charged Hayward black hole spacetime,” *Int. J. Mod. Phys. D* **29**, 2041014 (2020), arXiv:2005.13029 [gr-qc].

[86] T. M. Crispim, Marcos V. de S. Silva, G. Alencar, and Diego Sáez-Chillón Gómez, “Tidal stretching and compression in black bounce backgrounds,” *Eur. Phys. J. C* **85**, 1186 (2025), [Erratum: *Eur. Phys. J. C* 85, 1248 (2025)], arXiv:2507.00311 [gr-qc].

[87] M. Sharif and S. Sadiq, “Tidal Effects in Some Regular Black Holes,” *J. Exp. Theor. Phys.* **126**, 194–200 (2018).

[88] Eduardo Albacete and Maurício Richartz, “Tidal Forces in Majumdar-Papapetrou Spacetimes,” *Universe* **10**, 62 (2024), arXiv:2402.01634 [gr-qc].

[89] Marcos V. de S. Silva, T. M. Crispim, R. R. Landim, Gonzalo Olmo, and Diego Sáez-Chillón Gómez, “Tidal forces around the Letelier-Alencar cloud of strings black hole,” (2025), arXiv:2511.21604 [gr-qc].

[90] Dhruv Arora, Parth Bambhaniya, Dipanjan Dey, and Pankaj S. Joshi, “Tidal forces in the Simpson–Visser black-bounce and wormhole spacetimes,” *Phys. Dark Univ.* **44**, 101487 (2024), arXiv:2305.08082 [gr-qc].

[91] Haroldo C. D. Lima, Carolina L. Benone, and Luís C. B. Crispino, “Scalar absorption: Black holes versus wormholes,” *Phys. Rev. D* **101**, 124009 (2020), arXiv:2006.03967 [gr-qc].

[92] Haroldo C. D. Lima Junior, Carolina L. Benone, and Luís C. B. Crispino, “Scalar scattering by black holes and wormholes,” *Eur. Phys. J. C* **82**, 638 (2022), arXiv:2211.09886 [gr-qc].

[93] Haroldo C. D. Lima Junior, Renan B. Magalhães, Gonzalo J. Olmo, and Diego Rubiera-Garcia, “On the resolution of space-time singularities in spherically symmetric black holes: geodesic completeness, curvature scalars, and tidal forces,” *Class. Quant. Grav.* **42**, 225004 (2025), arXiv:2506.17918 [gr-qc].

[94] S. L. Shapiro and S. A. Teukolsky, *Black holes, white dwarfs, and neutron stars: The physics of compact objects* (Wiley-Vch, 1983).

[95] Wenkang Xin and Andrew Mummery, “The relativistic tidal tensor: general solutions for stationary axisymmetric spacetimes and the Hills mass of naked singularities,” (2025), arXiv:2511.21499 [gr-qc].

[96] Andrew Mummery, “The maximum mass of a black hole which can tidally disrupt a star: measuring black hole spins with tidal disruption events,” *Mon. Not. Roy. Astron. Soc.* **527**, 6233–6252 (2023), arXiv:2312.00557 [gr-qc].

[97] A. G. Abac *et al.* (LIGO Scientific, VIRGO, KAGRA), “GWTC-4.0: Updating the Gravitational-Wave Transient Catalog with Observations from the First Part of the Fourth LIGO-Virgo-KAGRA Observing Run,” (2025), arXiv:2508.18082 [gr-qc].